ORIGINAL PAPER

Damage to anthropic elements estimation due to large slope instabilities through multi-temporal A-DInSAR analysis

Martina Cignetti[1] · Danilo Godone[1] ⓘ · Davide Notti[1] · Francesco Zucca[2] ·
Claudia Meisina[2] · Massimiliano Bordoni[2] · Laura Pedretti[2] · Luca Lanteri[3] ·
Davide Bertolo[4] · Daniele Giordan[1]

Abstract

Deep-seated gravitational slope deformations (DsGSDs) are widespread phenomena in the Alpine environment. Their dynamics, although very slow, endanger human settlements and connecting infrastructures. Monitoring such phenomena is mandatory to evaluate the impact on infrastructure networks and inhabited areas. Nowadays, the implementation of a tool useful to define and manage the interactions of DsGSDs evolution and the anthropic element remains a challenge, particularly in land use planning. Apart from on-site monitoring, which is commonly poorly used for DsGSDs observation, satellite-based interferometry represents the most comprehensive instrument for an effective spatial and temporal characterization of these phenomena. This paper provides a dedicated procedure to assess the usability of Advanced Differential Interferometric SAR (A-DInSAR) techniques to explore the DsGSDs behaviour and investigate their local interaction along anthropic elements. Combining multi-temporal A-DInSAR data, ERS-1/2 (1992–2000), Radarsat-1/2 (2003–2010), COSMO-SkyMed (2011–2018) and Sentinel-1 (2014–2018), over the Motta de Pletè and Champlas du Col DsGSDs, north-western Italy, a line-of-sight displacement investigation over a long-time span is implemented. Multi-temporal deformation maps are generated to define the deformation pattern and DsGSDs evolution over time. Subsequently, a local-scale analysis along the main anthropic elements is performed, exploiting V_{slope} values and ground deformation time series, integrated with ground-based ones, where available. This local analysis is aimed to recognize the most critical sections of the anthropic elements along with an higher level of damage, and potential risk is expected. Moreover, the obtained results are compared with a survey damage of the anthropic elements for a local cross-check and to strengthen the A-DInSAR methodology. Overall, the presented methodology provides a powerful tool to better define the DsGSDs local dynamics in correspondence of the main strategic infrastructures and inhabited areas, for a proper infrastructure maintenance and territorial planning strategy.

Keywords Deep-seated gravitational slope deformation · Displacement · A-DInSAR · Infrastructures · Western Italian Alps

✉ Danilo Godone
danilo.godone@irpi.cnr.it

Extended author information available on the last page of the article

1 Introduction

Large slow-moving slope instabilities defined in the literature as Deep-seated Gravitational Slope Deformations (DsGSDs) (Agliardi et al. 2001, 2009; Pánek and Klimeš 2016) pose certain risks for human structures and infrastructures. Due to the long-term evolution of these phenomena that are characterized by a not-impulsive continuous deformation, the coexistence with anthropic elements is often possible, but damage to main infrastructures (e.g. roads, buildings, tunnels, penstocks, dams) is well-documented (Frattini et al. 2013; Béjar-Pizarro et al. 2017).

In the Alps, DsGSDs are usually characterized by a long-lasting evolution, with an occurrence referred to Late-glacial period, continuing during the Holocene until the present days. The progressive evolution of these phenomena can involve entire valley flanks, developing for hundreds of metres deep. Usually, the movement of DsGSDs is comparable to a slow creep, which sometimes can evolve into a local catastrophic collapse (Pánek and Klimeš 2016). Different factors influence the evolution of these massive phenomena, i.e. geological and structural features, tectonic and topographic conditions, glacial debuttressing, and seismicity (Martinotti et al. 2011; Crosta et al. 2013). This results in a complex evolution characterized by a varied displacement pattern, with distinct kinematic domains (Giordan et al. 2017; Frattini et al. 2018; Crippa et al. 2020), related to a differential rock mass strength degradation. Commonly, the upstream portions display long-linear morphological features like trenches, double-ridges, scarps, and counter-scarps, indicating an extensional regime. Conversely, the downstream portions show toe bulging, highly fractured rock masses poorly interlocked or completely collapsed, evidencing a compressive regime. The large progressive and cumulative displacement can also lead to secondary landslides (*e.g.* rockfalls, translational and rotational slides), mainly distributed in the middle and the lower portions of the slope, and characterized by a faster evolution.

In the Alpine range, DsGSDs are a widespread phenomenon (Mortara and Sorzana 1987; Ambrosi and Crosta 2006; Cignetti et al. 2020). In this mountainous territory, despite the high relief, there is an extensive urbanization and population compared to the other mountain areas of the world. The Alpine territory shows a significant human footprint and represents an important strategic hinge of Europe. In this mountainous area, DsGSDs are, by extension and gentle morphology, the ideal site of numerous inhabited centres and other strategic infrastructures, often exposing the anthropic structures and infrastructures to more or less severe damage. Damage can vary from slight effects, in urban areas without damage or crack to building walls, up to notable wall cracks and fractures (Di Martire et al. 2016), or road network interruption (Cignetti et al. 2019), up to cases where the decommissioning of a strategic work occurs (Barla 2018; Spreafico et al. 2020). An in-depth characterization of DsGSDs evolution, focusing on the higher strain domains, is a key element to recognize the urbanized areas more susceptible to damage, which is actually poor investigated both in risk management and land-use planning.

Among the remote sensing technologies, the Advanced Differential Synthetic Aperture Radar Interferometry (A-DInSAR) techniques (Ferretti et al. 2001; Berardino et al. 2002; Hooper et al. 2004) constitute a valid tool for ground deformation analysis of numerous phenomena, e.g. slope instabilities (Bordoni et al. 2018; Mantovani et al. 2019), volcanoes (Solaro et al. 2010; Traglia et al. 2021), earthquakes (Biggs et al. Valerio et al. 2018), subsidence (Bru et al. 2017; Solari et al. 2020b). In particular, these techniques are very suitable for slow-moving phenomena investigation as the DsGSDs (Colesanti and Wasowski 2006; Meisina et al. 2008; Cignetti et al.

2016; Bonì et al. 2018), through the measurement of surface displacement with millimetric accuracy, over wide areas, allowing analysis also of the areas with limited accessibility. Moreover, the increasing availability of multi-temporal satellite spaceborne acquisitions allows to a line-of-sight (LOS) displacement investigation over a long-time span. The A-DInSAR techniques have also been locally used for urban damage investigation commonly related to the evolution of the landslide (Ciampalini et al. 2014; Del Soldato et al. 2019a), while few are instead the cases in which such aspect is investigated on DsGSDs phenomena (Zangerl et al. 2010; Crippa et al. 2019). However, the application of these techniques in high mountain regions can represent a challenge, often making necessary to supplement this data with on-site instruments measurements (Giordan et al. 2013; Barboux et al. 2015; Wasowski and Pisano 2020; Allasia et al. 2020a). In addition to the intrinsic limitation of the DInSAR techniques (i.e. LOS measurement only, coherence loss due to long revisit time, phase decorrelation due to large or rapid displacement, the complex orography that causes unsuitable valley flanks orientations relative to the SAR view angle), other limitations must be considered. In particular, in the mountainous region, the main issues are primarily due to the abundant vegetation or snow cover that can affect the temporal correlation of the signal, and the atmospheric disturbance amplified by high topography gradient. Part of these problems can be forecasted and mitigated with some methodologies such as pre-processing data feasibility (Bordoni et al. 2018; Del Soldato et al. 2021) or the projection of the velocity along the slope (V_{slope}) (Notti et al. 2014).

In this paper, two representative active DsGSDs of the Western Italian Alps have been analysed, focusing on their interaction with the main existing anthropic elements. Leveraging on the available A-DInSAR datasets, a general overview of the damage and the level of damage to the main structures and infrastructures are examined. Two DsGSDs, with distinct behaviour, are investigated: (1) Champlas du Col, Sestriere, Piemonte Region, Italy; (2) Motta de Pleté, Breuil-Cervinia, Aosta Valley Region, Italy. We first made a PS (Permanent Scatterer) feasibility analysis including SAR datasets examination, concerning the assessment of the main characteristics of the available SAR datasets. Then, we carried out a post-processing on multi-temporal SAR data acquired by the different sensors, concerning the assessment of DsGSDs detectable movement in terms of percentage and the reliability of the measurement, taking into account of the percentage of detectable ground motion and the target distributions (Notti et al. 2014). Specifically, exploiting multi-temporal A-DInSAR data (ERS-1/2, RADARSAT, COSMO SkyMED, Sentinel-1), V_{slope} maps and ground deformation time series, for 26–28 years are generated and integrated with on-site measurements, where available, in order to: (1) study the selected DsGSDs to characterize their deformation pattern and evolution, (2) perform a local-scale analysis of the main anthropic elements (because of the distinct evolution of each phenomenon), through the subdivision of the main infrastructures and inhabited centres into homogeneous sections, based on the V_{slope} values. In addition, the obtained data are compared with the observations of the damage from on-site investigations. In this way, the in-depth characterization of the various anthropic elements in terms of potential damage and degree of damage are obtained. The final goal of the proposed methodology is implementing an innovative procedure suitable for estimating impacts of DsGSDs on infrastructures and identifying most critical sectors, providing an effective tool for a more efficient and effective definition of ad hoc in situ monitoring solutions and maintenance plants.

2 Area of interest

The Western Italian Alps, despite the abrupt terrain characterized by steep slopes, is one of the most urbanized mountain environment in the world (ISTAT 2019). The alpine landscape represents an environmental and cultural heritage, with a strong anthropic footprint, and a strategic and economic hinge in the European scene. Due to the combination of complex lithological and structural setting and high relief energy, the Western Italian Alps (WIA) reveal a notable exposure to slope instabilities. Landslides vary in type and size, ranging from punctual rockfalls to large slope instabilities. Referring to the Italian National Landslide Inventory (i.e. IFFI, *Inventario Fenomeni Franosi Italiano*, Trigila et al. 2008), 799 DsGSDs are catalogued, affecting about 8% of the WIA territory. The most affected areas are the Aosta Valley Region (AVR) and the Province of Turin (located in the Piemonte Region), specifically in the Susa, Chisone and Pellice Valleys in the middle-low portion of the province. By focusing on these areas, highly affected by active DsGSDs, two case studies were selected (Fig. 1): (1) Champlas du Col (CDC) DsGSD, Chisone Valley, Piemonte Region (2) Motta de Pletè (MDP) DsGSD, Valtournenche, Aosta Valley Region.
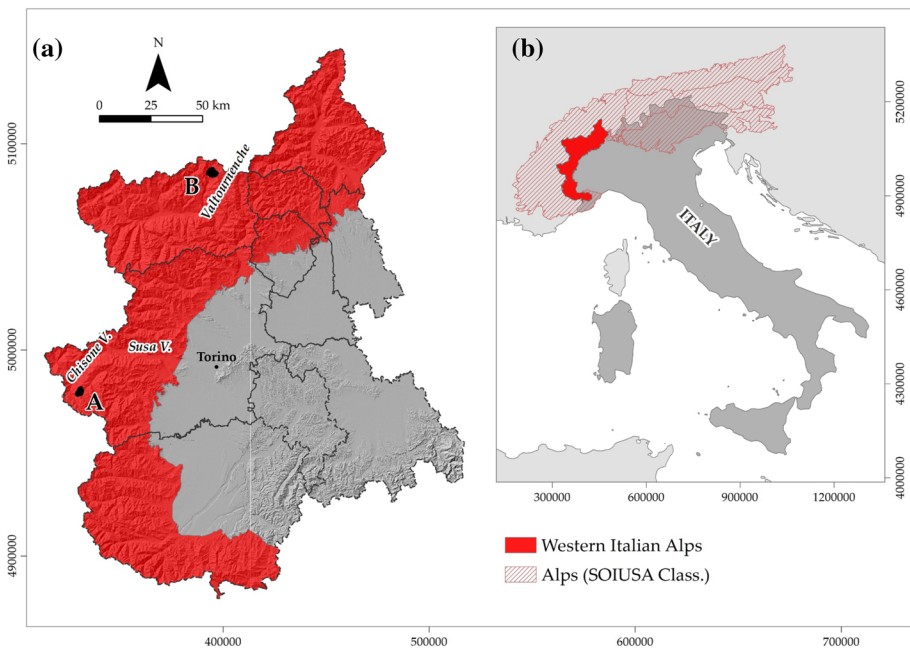

Fig. 1 Location of the area of interest: **a** Italian Western Alps (red polygon) with the selected case studies (A) Champlas du Col DsGSD, (B) Motta de Pletè DsGSD, Aosta Valley Region; the dashed dark grey lines represent the provincial limits of the two regions; **b** European Alp SOIUSA classification (Marazzi 2005) in dark red the Western Alps Italian side

3 Geological and geomorphological setting

3.1 Champlas du Col

The Champlas du Col (CDC) DsGSD is located in correspondence with the Upper Susa watershed and the Chisone Valleys (northern Cottian Alps), close to the Sauze di Cesana and Sestriere villages, renowned mountain tourism and ski resorts localities. The CDC DsGSD is an active phenomenon, extended for about 5,1 km², involving the entire slope from the Mt. Fraiteve (2700 m a.s.l.) to the Ripa Torrent. In the middle-low portion, this large slope phenomenon is crossed by the national road (Provincial road n°23) that connects the Champlas du Col hamlet with Sestriere (Fig. 2).

The geological setting of this area is represented by the oceanic units of the "*Lago Nero*" (LN) unit, mainly represented by undifferentiated calcschists, micaceous marbles and phyllites, and by the metasedimentary sequence of calcschists of the "*Cerogne-Cian-tiplagna*" (CC) unit, belonging to the Pennidic system (Fioraso 2017). The bedrock of the CDC DsGSD is mainly represented by the calcschists of the CC unit, while the LN unit outcrops just in the upper part of the DsGSD.

Morphologically, the CDC DsGSD is characterized by poor surficial evidence of deformation, mainly represented by some counterscarps, and by the main scarps that border the Granges des Alpes plain. The lack of linear morphostructural features, characteristic of DsGSDs phenomena, is primarily due to the pervasive interference with numerous secondary landslides and the vast detrital deposits. Specifically, in the middle-low portion of the slope, numerous secondary slope failures (e.g. complex landslides, rotational and translational slides) superimposed to the DsGSD, reshape the slope (Cignetti et al. 2019).

In correspondence of the Champlas du Col and Champlas Janvier villages, several inclinometers are distributed upstream and downstream of the S.P.23, associated with some piezometers and GNSS benchmarks. The inclinometer network acquired data from November 2001 until Jun 2010. The most remarkable displacement (19 mm/year, 24 mm/year) was recorded at about 30 m depth by two inclinometers located upstream the building area of Champlas du Col. It is worth noting that relevant damage were observed in correspondence of the walls-structures of several buildings in the Champlas du Col and Champlas Janvier villages (Drago et al. 2012), with a punctual damage description and classification. Moreover, considerable fractures of the S.P.23 road surface due to a secondary landslide reactivation (Cignetti et al. 2019) were recorded over time, until the road interruption in the May 2018 reactivation.

3.2 Motta de Pleté

The Motta-de-Pleté DsGSD is located in the upper part of Valtournenche (Pennine Alps), close to Breuil-Cervinia, another renowned ski resort, in the Aosta Valley Region. This active phenomenon extends for about 8 km², involving the entire slope from the Motta-de-Pleté Oriental peak (3016 m a.s.l.) to the Marmore Torrent. In the north-western limit, this large gravity-induced phenomenon highly affects the Cielo-Alto locality, a small resort consisting mainly of hotels and buildings for tourist use. Moreover, the MDP DsGSD variably interferes with a penstock extended from the Perrères hydroelectric station, located on the north-eastern sector of the DsGSD, up to the Goillet Reservoir (Fig. 3).

From a geological point of view, the bedrock is composed of the rocks belonging to the Piedmont Nappe System, here represented by the Zermatt-Saas Unit, mainly
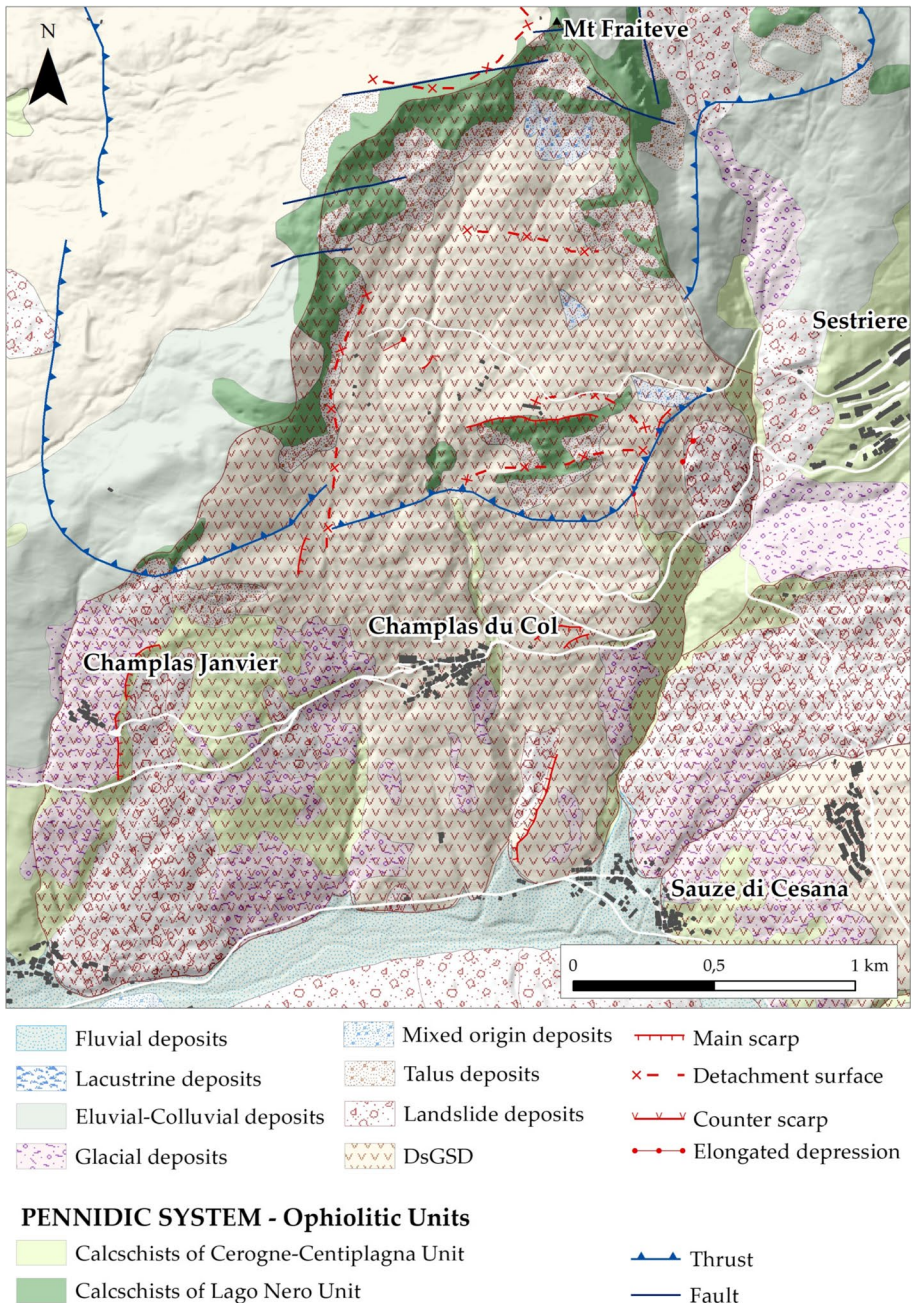
Fig. 2 Geological map of the Champlas du Col case study [revised from (ISPRA CARG 2006)]

composed of serpentinites, serpentineschists and metabasites, and the Combine Unit or Tsaté Unit, mainly represented by calcschists and prasinites, separated by the Pancherot—Cime Bianche Unit, consisting of quartzites, dolomitic marbles, calcareous marbles,
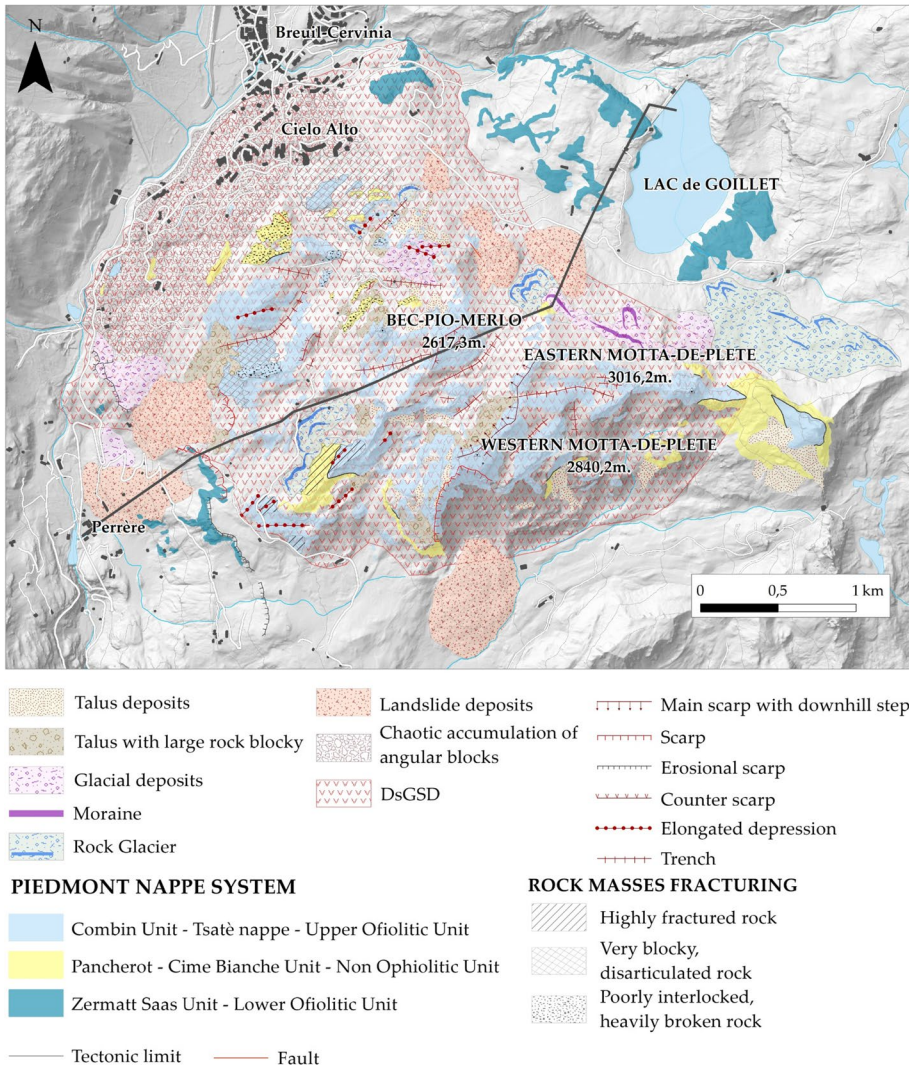
Fig. 3 Geological map of the Motta-de-Pléte case study [revised from (Giordan 2006)]

pseudocarnioles and evaporites (CARG ISPRA 2015). Only the Combine Unit are affected by the DsGSD, as testified by the surveys and drilling achieved for the Perrères hydroelectric station (Martinotti et al. 2011).

Morphologically, the MDP DsGSD is characterized by a hummocky topography, extended rock glaciers and moraine ridges, highlighting a primarily periglacial environment. Numerous linear morpho-structural features characterize the entire slope. An important scarp extended from the Central to the Western Motta-de-Pleté peaks, corresponds to a listric fault that causes the rotation of a calcschist block (Martinotti et al. 2011), which forms an evident counter scarp. The whole upper portion of the DsGSD is characterized by trenches, elongated depression, deep fractures and karst cavities, testifying an extensional regime. Moving downstream, the rock outcrops display a progressive increase in

fracturing. From Bec Pio Merlo peak (2617 m a.s.l.), the slope displays a jagged steps profile and fractured blocky rocky outcrops. Proceeding to Cielo-Alto locality, the rocky outcrops become poorly interlocked up to heavily broken rock masses collapsed onto themselves, indicating a domain highly involved in the gravitational phenomena where damages to numerous hotels and buildings have been observed.

4 Materials and methods

The presented methodology aims to implement a useful tool for a rapid definition of the impact of DsGSDs on infrastructures, an aspect generally lightly considered and underestimated in risk management and land-use planning that, however, can pose a certain risk due to the long-lasting deformation of these huge phenomena. The implemented methodology is mainly based on the use of A-DInSAR techniques, integrated, where available, with on-site instruments, (Fig. 4). Leveraging on the advantage of multi-temporal A-DInSAR, the evolution and behaviour of the selected active DsGSDs are analysed and characterized. In particular, the velocity along the steepest slope and the E–W and vertical components are computed by post-processing the available SAR datasets. Once the characterization at the slope scale was carried out, the methodology provides for the analysis, at local scale, of the main anthropic elements, of the area of interest.
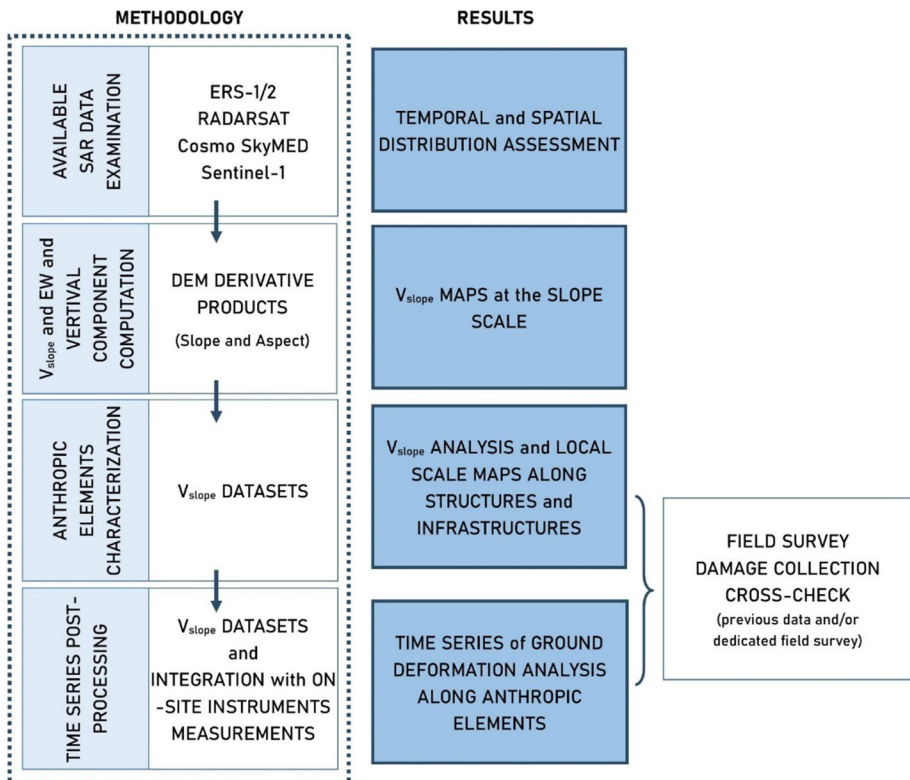

Fig. 4 Workflow of the implemented methodology

Once the structures and infrastructures have been identified, they have been subdivided into homogeneous portions. This characterization is based on the V_{slope} values analysis and functional for identifying the sectors potentially subject to damage. Jointly, the assessment of deformation time series (TS) is performed, and, where available, the SAR TS are integrated with on-site instruments measurements.

In addition, a comparison between V_{slope} maps and the damage type observed on the field and their level of severity is performed, to locally cross-check the obtained results and discuss the usability of the methodology as well as applying it in other similar areas.

4.1 Available interferometric dataset

The growing availability of multi-temporal satellite space-borne acquisitions allows to an increasing use of A-DInSAR techniques to analyse the spatial and temporal evolution of slope instabilities (Herrera et al. 2013; Bonì et al. 2018; Solari et al. 2020a), and in particular of extremely slow phenomena as the DsGSDs (Di Martire et al. 2016; Frattini et al. 2018; Antonielli et al. 2019).

For the selected areas of interest, diverse SAR datasets are available (Table 1). It should be noted that the existing SAR datasets were provided by two different Regions with distinct administrations. Therefore, the PR and AVR provide diverse datasets with different temporal coverage. Specifically, we used data from ERS-1/2 (ERS), Radarsat-1/2 (RSAT), COSMO-SkyMed (CSK) and Sentinel-1 satellites (Table 1). The data cover the temporal range 1992–2018 for PR and 1992–2020 for AVR. The ERS data were processed with the PSInSAR™ technique (Ferretti et al. 2001). The CSK data for PR were processed by the Italian Space Agency (ASI) in the framework of the "Piano Straordinario di Telerilevamento" (PST) (http://www.pcn.minambiente.it/mattm/en/project-pst-interferometric-products/), while for the AVR were processed by the TRE-Altamira group. The other datasets were processed with SqueeSAR™ technique (Ferretti et al. 2001).

Considering the areas of interest, a certain difference in the number of PSs is observable between datasets (Table 2). This variance is mainly due to the revisit time of the satellites,

Table 1 Overview of the main SAR dataset (A) ascending geometry, (D) descending geometry, of Piemonte (PR) and Aosta Valley (AVR) regions

Satellite	ERS-1/2	RSAT	CSK	Sentinel-1
Band	C	C	X	C
Incident angle (°)	23° (A) 23° (D)	35° (A) 34° (D)	P 32°—AVR 29° (A) P 30°—AVR 27° (D)	P 35°—AVR 38° (A) 43° (D)
Revisit time (days)	35	24	4–16	6–12
Period (month/year)	04/1992–12/2000	04/2003–10/2010	P 05/2011–04/2014 AVR 01/2015–05/2018	P 2014–2018 AVR 10/2014–05/2020
N° images	PR 36 (A) 77(A) AVR 50(A) 86(D)	PR 77(D) 76 (A) AVR 101(A) 94(D)	PR 40(A) 40(D) AVR 67(A) 64(D)	PR 165(D) 174(A) AVR 248(A) 253(D)
Spatial resolution (m)	30	28	3	5×20
Processing	PSInSAR™	SqueeSAR™	P: PST-ASI AVR: SqueeSAR™	SqueeSAR™

Table 2 SAR data information within the selected case studies

Area of interest	Dataset	PS number	Density (PS/ha)	Mean nearest neighbour distance (m)
CDC	ERS A	14	0.025	165
	ERS D	56	0.101	63
	RSAT A	147	0.266	51
	RSAT D	145	0.263	64
	CSK A	3058	5.542	4
	CSK D	947	1.716	3
	Sentinel A	877	1.589	27
	Sentinel D	734	1.330	28
MDP	ERS A	57	0.061	56
	ERS D	93	0.099	18
	RSAT A	110	0.117	22
	RSAT D	102	0.109	16
	CSK A	78	0.083	11
	CSK D	72	0.077	7
	Sentinel A	261	0.279	34
	Sentinel D	266	0.284	27

as in the ERS-1/2 case, in which the low number of images highly impacts the quality of the dataset compared to the others one, particularly in the PR case study.

The PS number in the four datasets and their distribution varies considerably (Table 2), mainly due to some intrinsic limitations of the DInSAR techniques (i.e. unsuitable valley flank orientation to sensor view angle, line-of-site (LOS) measurements only, coherence loss due to large revisit time, temporal decorrelation effects due to high-vegetated areas) (Colesanti and Wasowski 2004; Cascini et al. 2010). Low data coverage in the four datasets is mainly due to land use with high-vegetated areas, mainly represented by forests and pasture, covering almost half of the DsGSDs. Only in correspondence of the principal urbanized areas, e.g. Champlas du Col hamlet and Cielo Alto locality, a good SAR data distribution is observed. The mean nearest neighbour distance (Table 2), calculated as the mean of the distances from each point to its nearest neighbour, well-represents the PS/DS distribution of the case studies for each dataset.

4.2 Calculation of the vertical and E–W components and projection along the slope

The A-DInSAR techniques ensure to detect the ground deformation velocity along the line of sight (LOS) of the satellite. Using different satellites, the detected movement is variable and depends on the different SAR acquisition geometries (Plank et al. 2012) and on the morphological characteristics of the area (i.e. slope, aspect). Therefore, in order to make a comparison between phenomena with diverse slope aspect and to homogenize different datasets derived from satellites with distinct incident angles, a post-processing procedure is required (Colesanti and Wasowski 2006; Bianchini et al. 2013; Bonì et al. 2018). We use the post-processing methodology and equations, described in Béjar-Pizarro et al. (2017), Notti et al. (2014), Raspini et al. (2012), to

project the V_{LOS} along the maximum slope gradient (V_{slope}) and to resolve the east–west (V_{E-W}) and vertical (V_H) components of velocity.

The average velocity along the steepest slope has been computed according to Eqs. (1) and (2).

$$C = \{N * \text{COS}\,[s * \sin(a-90)]\} + \{E * [-1 * \text{COS}(s) * \text{COS}(a-90)]\} + [H * \sin(s)] \tag{1}$$

$$V_{slope} = V_{LOS}/C \tag{2}$$

where $H = \text{COS}(\alpha)$; $E = \text{COS}(90-\alpha) * \text{COS}(270-\gamma)$; $N = \text{COS}(90-\alpha) * \text{COS}(180-\gamma)$; $\alpha = $ LOS incidence angle; $\gamma = $ LOS azimuth; $s = $ slope; $a = $ aspect.

According to previous studies (Notti et al. 2014; Bonì et al. 2018), the proposed procedure assumes that the main movement occurs along the steepest slope, comparable with a translational kinematic. This implies that in cases with predominant rotational movement, the percentage of detectable movement can be underestimated, based on the value of the C index used. In the proposed methodology, all PSs with $-0.2 < C < 0.2$ are discarded to avoid exaggerating the projection error (e.g. with $C = 0.2$, the standard deviation of velocity is five times greater). Moreover, the PSs with $V_{slope} > +2$ mm/year were removed, considering a positive value not a reliable from a geomorphological point of view.

The V_{slope} is calculated from slope and aspect derived from the regional 10 m DEMs, made available from regional authorities, and only the PS/DS with a slope gradient greater or equal to 5° were projected. It should be noted that the local topography and its variations in slope orientation, especially where terrain shows hummocky geomorphology (e.g. counter slope, trench), may affect the C values coefficient (Notti et al. 2011), a question reducible through the use of a rougher digital terrain model. However, due to the above mentioned limitations, the use of V_{SLOPE} should be associated, when available, with some ground measures of the direction of movement, derived from on-site instruments, in order to harder the satellite-derived movements and validate the obtained results. Unfortunately, traditional instruments and on-site monitoring network are rare for deep and slow-moving phenomena such as DsGSDs, for which often only satellite-derived data are available.

Subsequently, using the interpolated velocity of descending (V_{LOSd}) and ascending (V_{LOSa}) datasets (Notti et al. 2014), we obtained the east–west component (V_{e-w}) and the vertical (V_H), from Eqs. (3) and (4), respectively.

$$V_{e-w} = \left[(V_{LOSd}/H_d) - (V_{LOSd}/H_a)\right] / (E_d/H_d - E_a/H_a) \tag{3}$$

$$V_H = \left[(V_{LOSd}/E_d) - (V_{LOSd}/E_a)\right] / (H_d/E_d - H_a/E_a) \tag{4}$$

where $H = \text{COS}(\alpha)$; $E = \text{COS}(90-\alpha) * \text{COS}(270-\gamma)$; $\alpha = $ LOS incidence angle; $\gamma = $ LOS azimuth.

We finally joined, for each satellite, ascending and descending geometries: if both of them converge to a similar value of V_{slope}, it means that the dataset has good accuracy, and the velocity is close to the ground truth (see supplementary material for details). In our study cases, we projected seven datasets along the slope. Only the descending dataset of CSK for Piemonte case and CSK ascending for Aosta Valley were discarded because of their anomalous V_{LOS} value (slight shift or noise not detectable until local analysis) in the original processing. The resolved components of velocity were obtained for Sentinel-1 and RSAR datasets, while it was not computed for ERS-1/2 due to the low density of PS.

5 Analysis of the anthropic elements

The detection of the principal lines of communication (i.e. road, railway), the identification of the main built-up areas and other strategic infrastructures like penstocks, is essential to a clear definition of the interaction of DsGSDs with the main anthropic elements. Operating in an open-source geographic information system (GIS) (QGIS Development Team 2009), through selection and intersections tools, the analysis of the interaction between DsGSD polygon and the anthropic elements in vector format is easily achievable.

For the areas of interest, we consider the vector data derivable from the regional technical map (e.g. CTR), for both PR and AVR cases. The principal elements correspond to provincial roads, small towns and hamlets, which are all renowned mountain tourist places, and penstock of hydroelectric plant.

Subsequently, a characterization of each structure and infrastructure selected is provided in the implemented methodology in order to define the most critical sectors. Leveraging the available SAR datasets, we operated by characterizing each anthropic element in homogeneous portions based on V_{slope} values of the PS/DS located above and within a reasonable vicinity of artificial features. Regarding linear elements such as road or penstock, we applied a buffer of 10 m, thus including a portion of territory along with the linear structures relevant for the scopes of the analysis. Instead, for the urbanized areas, to get the influence zone of each PS/DS, we operated by combining an interpolation tool, i.e. Natural Neighbors (Godone and Garnero 2017), and the Voronoi Diagram (Gold 1994), to obtain a spatial subdivision of the area and minimize the subjectivity of the operator. The polygons obtained by merging the two methods were manually checked to edit minimal feature and optimize polygon significance.

In the anthropic elements characterization phase, portions without PS/DS were distinguished and classified as "No Data". Instead, the other portions were classified by attributing velocity ranges of the average V_{slope} calculated from the PS/DS available on each section.

We considered, as a reference to define the areas, the CSK dataset, for the PR case study, and RSAT for AVR one. These datasets, respectively, represent the best coverage and distribution of SAR data, also showing the optimal SAR data coverage on anthropic elements. Subsequently, the analysis was done for the other three datasets available. In this way, a comparison of the SAR datasets has been possible, leading to identifying those portions with higher velocity and possible spatial and temporal velocity variations along the main structures and infrastructures over time.

6 Time series post-processing and analysis

The subsequent step is devoted to perform the time series (TS) of SAR data to analyse the ground deformation close to the most critical portions of the anthropic structures and infrastructures previously identified. The objective is to obtain historical series as continuous as possible over time, also integrating measurements acquired by the diverse available sensors. Moreover, the use of external data is expected for those sectors where on-site instruments measurements are available.

Before interpreting the data, it is necessary to carry out some post-processing to assess TS quality. The first step is to check if all the TS is affected by systematic bias or outliers

related to processing. In a second step, the TS of the selected area is averaged to smooth the noise of a single TS to help the identification of potential trends.

We projected the TS along the slope using Eqs. 1 and 2 to compare InSAR with TS from other instruments. We also computed the total displacement for the whole period (1992–2020) by summarizing and joining, through linear regression, the time series of each period/satellite.

7 Results

7.1 DsGSD phenomenon scale analysis

For each case study considered, the map of the LOS velocity projected along the slope (V_{slope}), to make them comparable, is generated for each available SAR dataset. We also generate the maps of the E–W and vertical components, in cases where ascending and descending data allowed for it. Full data for CDC and MDP cases for each SAR dataset available can be found in the Supplementary Materials.

In the CDC DsGSD, the velocity maps are strongly influenced by slope orientation and the PS/DS density of each dataset (Fig. 5). The slope orientation north–south causes strong variation of C index and, as a consequence the V_{slope} has abrupt variation and outliers values caused by a change of just a few degrees in the aspect. The filters allowed to limit the outliers and the V_{slope} values of the four datasets agree at the DsGSD scale (Fig. 5E). The SAR data density for ERS and RSAT allowed having data only for the small villages, while CSK and Sentinel-1 show widespread distribution. The resolving of the velocity in the E–W and Vertical vectors showed a good agreement with slope orientation: PSs on SSW slope show a weak west velocity component, while weak East is predominant on the PSs on SSE slope. Despite these limitations, it is possible to note, especially with Sentinel-1 and CSK data, a variability of the movements across different portions of this DsGSD. In particular, the moving PSs are concentrated in the central and in the upstream portions of this huge phenomenon, allowing to distinguish a sub-domain characterized by a velocity rate higher than the downstream sector of the DsGSD. In addition, the contribution related to secondary landslides that characterize the downstream portion of the investigated phenomenon should be considered. For instance, the complex landslide near Champlas Janvier or the zone at NE of Champlas du Col hamlet, which shows a 20 mm/year movement, are clearly identifiable.

Concerning the analysis of the V_{slope} of the MDP DsGSD, we observed an average value of 5 mm/year, for ERS, RSAT and Sentinel-1 datasets (Fig. 6A, B, C, E). The E–W component, based on Sentinel-1 data (Fig. 6D, E) shows a mean value of 3 mm/year towards west, in agreement with slope orientation to NW, while the vertical component ranges about 2–3 mm/year downslope. The CSK dataset, which covers almost the same period of Sentinel-1, is not reported in the figure but shows a similar value of V_{slope} (Supplementary material). The hummocky morphology of this DsGSD, with many trenches and counter slopes, could have locally disturbed/biased the velocity projection, even if it is filtered. It is possible to see on the maps (Fig. 6) that there are areas with higher velocity, mainly in the north and western part of DsGSD. In detail, observing the penstock and the Cielo Alto village areas, the V_{slope} velocity range is about 10–15 mm/year, and the E–W velocity is about 5–10 mm/year.
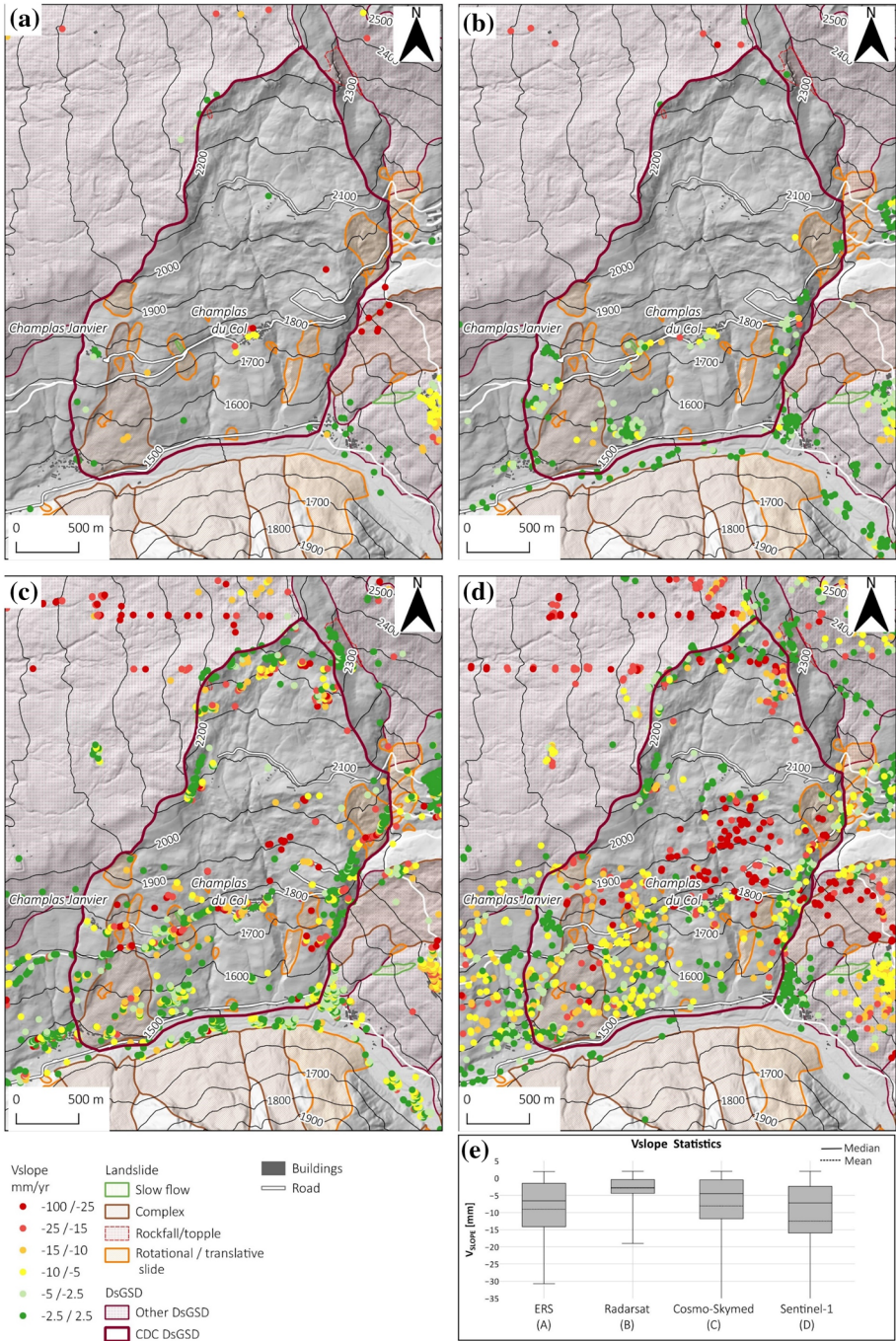
Fig. 5 V_{slope} maps of the CDC DsGSD in **A** ERS, **B** RSAT, **C** CSK, and **D** Sentinel-1 datasets. **E** Box plot diagram of V_{slope} for ERS (A), Radarsat (B), CSK (C) and Sentinel 1(D) distribution for the PS/DS located inside the whole DsGSD boundary
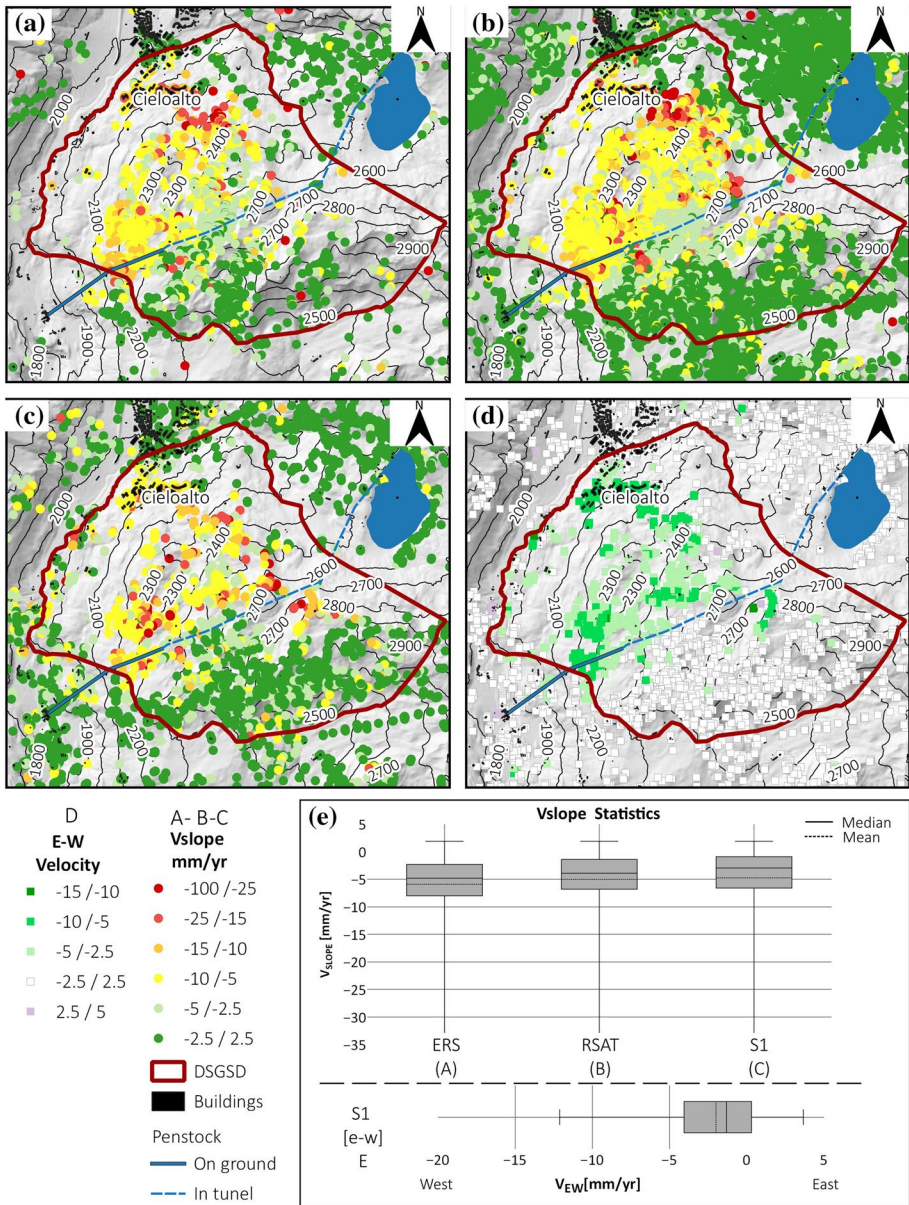
Fig. 6 The V_{slope} map of MDP DsGSD based on ERS (**A**), RSAT (**B**) and Sentinel-1 (**C**) data. **D** E–W velocity map based on Sentinel-1 data. **E** Box plot diagram of V_{slope} for ERS (A), Radarsat (B), Sentinel-1 (C) and V_{EW} (D) distribution for the PS/DS located inside the whole DsGSD boundary

7.2 Anthropic elements characterization

The analysis of the V_{slope} distribution within the studied DsGSDs allows us to identify those sectors with a high velocity that often interfere with the main anthropic elements

crossing these huge phenomena. Therefore, operating through a V_{slope} values analysis, we characterized the structures and infrastructures intersecting the CDC and MDP DsGSDs. In particular, the distribution of the average of the V_{slope} variable along the various linear artificial features and the urbanized areas allows distinguishing sectors with higher deformation and their variation over time.

For the CDC DsGSD, the principal anthropic elements correspond to a stretch of provincial road (SP23) that intersects the phenomenon in the central sector, and the Champlas du Col hamlet crossed by the aforementioned road. Figure 7 shows the SP23, the main connection between Champlas du Col hamlet and Sestriere, divided into sections with homogeneous V_{slope}. In general, the V_{slope} values are rather variable, mainly due to the high variability of the slope's topography characterized by frequent slope exposure changes. The upstream sectors in correspondence with the bifurcation of the SP23 within the Champlas du Col hamlet, and some portions along with the two hairpin bends, display the higher velocity deformation, with a mean V_{slope} range variable from − 20/− 15 up to − 100/− 40 mm/year.

Examining the trait of road adjacent to the NNW sector of the urbanized areas, i.e. close to the cemetery of Champlas du Col, we detected a constant velocity range of − 40 – 20 mm/year on all the four datasets, covering a time span from 1992 to 2018.

Observing the CSK (Fig. 7C) and Sentinel-1 (Fig. 7D) data, in correspondence of the portions along with the two hairpin bends display the highest velocity deformation, ranging from – 40 to − 20 and – 100 to − 40 mm/year, close to the small slide reactivated during the 2018 spring (Cignetti et al. 2019).

Focusing on the urbanized area of Champlas du Col (Fig. 8), we observed, for the available datasets, a general decrease in V_{slope} range from west to east, with the highest velocity in correspondence of the area close to the cemetery. The values of the average V_{slope} of this area, corresponding to the north-west limit of the inhabited centre, are almost constant across the available datasets, ranging from − 20 mm/year up to − 36 mm/year.

For the MDP DsGSD, the principal anthropic elements correspond to the Cielo Alto touristic locality, close to the Breuil-Cervinia village at the limit of the DsGSD, and the surface section of the penstock of the Perrères hydroelectric plant, at the southern limit of the DsGSD. The urban area of Cielo Alto presents V_{slope} values rather homogeneous throughout the built-up area, ranging from − 5 to − 10 mm/year. Figure 9 shows the V_{slope} homogeneous areas for the RSAT dataset, almost constant on the other datasets (maps available in Supplementary material).

Proceeding upstream, we recognize sectors with higher velocities, varying progressively from – 10 to − 15 mm/year up to a peak of – 25.5 mm/year in the ENE sector of the locality. Along the DsGSD limit, the V_{slope} decreases considerably, with general stability in correspondence of Breuil-Cervinia.

Concerning the penstock located in the south-western limit of the DsGSD, the infrastructure was subdivided into three main traits. A small portion, just downstream the DsGSD limit, shows no SAR data coverage due to the forest canopy cover. Considering as reference the RSAT dataset (Fig. 10), the V_{slope} values in the recognized traits remain almost constant in the available datasets (maps in Supplementary material), with a velocity of about − 10 mm/year. Proceeding towards the Perrères hydroelectric plant, a general decrease in velocity rates is observed up to a general stability at the valley bottom.
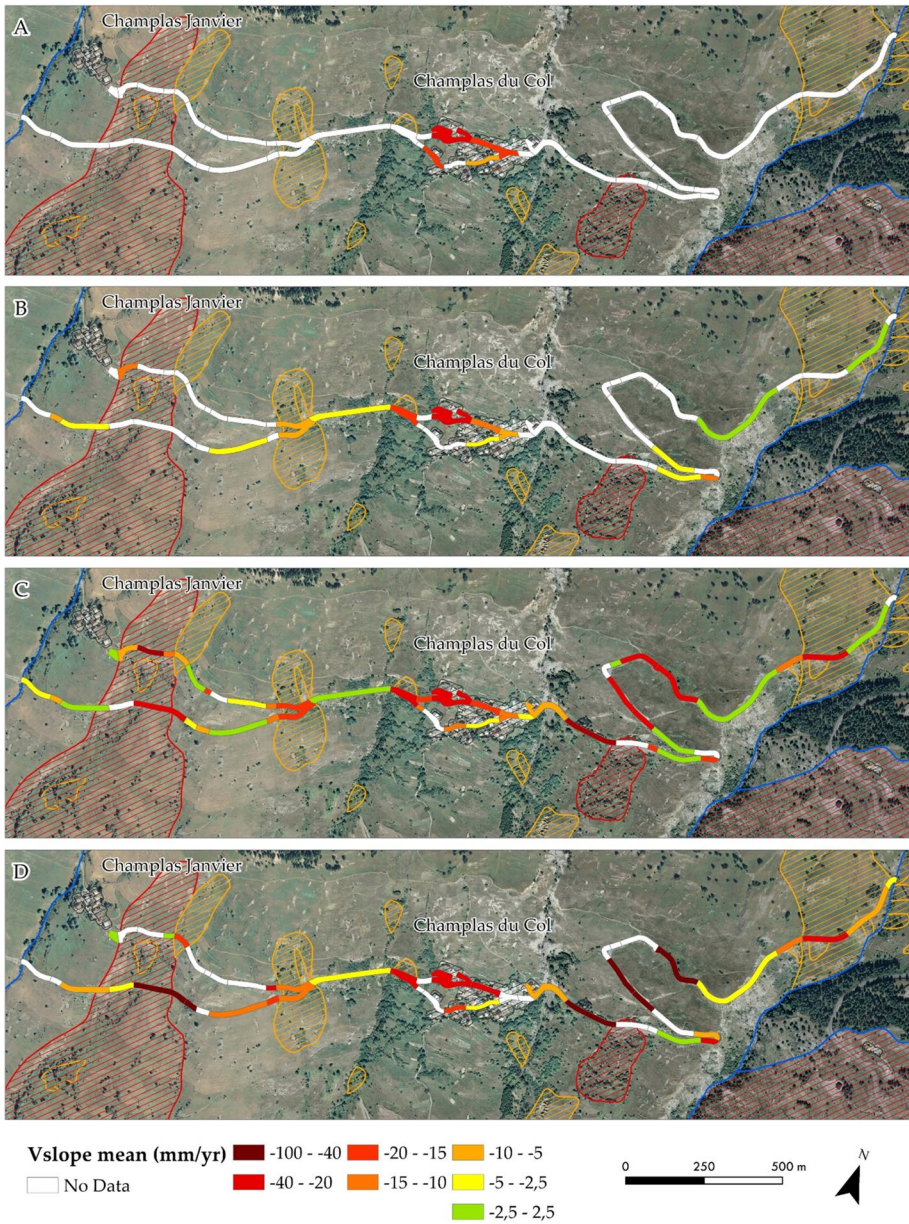
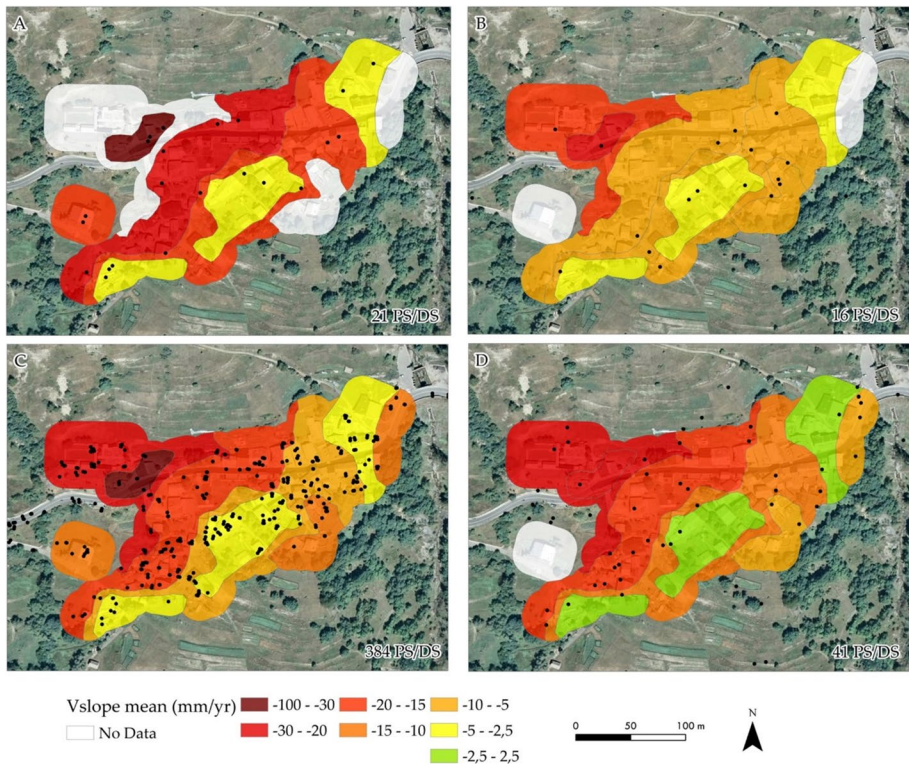**Fig. 7** SP23 road in the middle sector of the CDC DsGSD subdivided into homogeneous sections based on the V_{slope} values compared in the **A** ERS, **B** RSAT, **C** CKS and **D** Sentinel-1 datasets

7.3 Structures and infrastructures time series analysis

Recognized the areas more critical along infrastructures and inhabited areas, in correspondence of these sectors ground deformation A-DInSAR time series are generated and analysed. In general, we analysed the time series of all satellites; however, only Sentinel-1

Fig. 8 Champlas du Col hamlet subdivided into homogeneous areas based on the V_{slope} values compared in the **A** ERS, **B** RSAT, **C** CKS and **D** Sentinel-1 datasets. The black points correspond to the PS/DS distribution for each dataset

satellites, thanks to their high revisit time (Table 1), and low noise allowed us to make a more accurate analysis of displacement. Moreover, where on-site measurements were available, an integration with A-DInSAR TS was carried out.

For the CDC case study, Fig. 11A shows the section of the road SP23, close to the rotational landslide reactivated in May 2018 (Cignetti et al. 2019). We show only the time series of Sentinel-1 because both their quality (e.g. PS density and distribution) and temporal span (revisit time of 6 days) are much better than CSK and RSAT data. We first averaged the time series of all PS and DS located nearby the buffered polygons of roads. Then we compared InSAR displacement with snow depth because, according to a previous study (Cignetti et al. 2019), its melting is the main trigger of acceleration events. We can observe from panels B and D of Fig. 11 some shreds of evidence. The TS presents noised data during the snow coverage periods and the noise increase with the depth of snow. Another factor that should be considered is the frequency of acquisitions that increased from 12 to 6 days from the summer of 2016 when both Sentinel-1 satellites became operative. We calculated the V_{LOS} for the snow-free periods (May–November) from 2015 to 2018, and it is possible to observe a relationship with the snow depth of the previous winter. In 2018 when the snowpack on the ground reached 180 cm and the total cumulated snow of winter 600 cm, the LOS velocity reached 25 mm/year. While in the winters 2014/2015 and 2015/2016, smaller snow coverage corresponds to slower velocity. On short time intervals
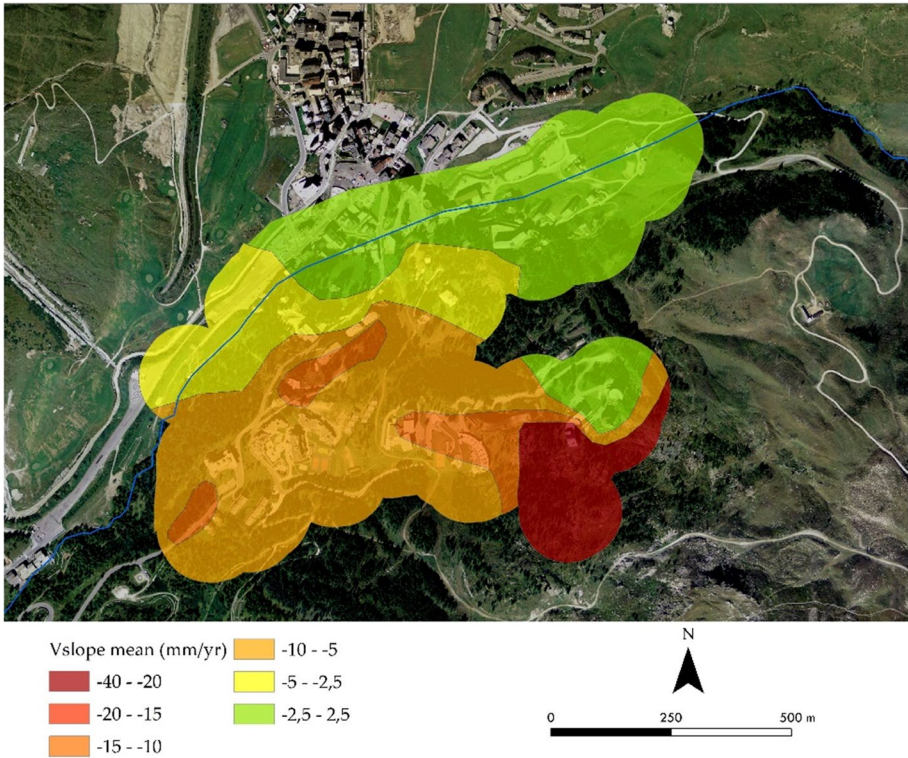
Fig. 9 Urbanized areas of the MDP DsGSD subdivided into homogeneous areas based on the V_{slope} values compared in the RSAT dataset

(e.g. 2 months), the calculation of the partial velocity could be affected by more noise. However, it is possible to observe that most accelerations occur in the first months after snow melting (May–June). If projected along the slope, these partial velocities are at least three times faster than V_{LOS}, so the absolute acceleration of 2018 probably reached the 100 mm/year in the road segment just west of the 2018 landslide (Fig. 11). The abrupt acceleration like the one that occurred in May 2018 (Fig. 11A) are too rapid to be detected by InSAR and no data are available.

In the CDC village (Fig. 11C), a comparison between the Sentinel-1 time series (Fig. 11D), projected along the slope, and the in-place inclinometer of (ARPA Piemonte 2021) has shown a similar trend despite the noise related to projection. Inclinometer data showed two sliding surfaces at 18 and 30 m from the surface. Also, in this case, the acceleration after the snowy winter 2017–2018 is evident. The snow noise effect on time series could be observed in most of the dataset and it is more evident on DS rather than PS.

For the MDP DsGSD, we analysed the averaged TS of SAR data located on the buildings of Cielo Alto (Fig. 12A) and the section of the penstock most affected by movement (Fig. 12C). For all datasets analysed it is possible to observe an almost linear trend both for Cielo Alto and penstock (Fig. 12B, D). Over the monitoring period (1992–2020) the total displacement is about 300 mm (projected along the slope).
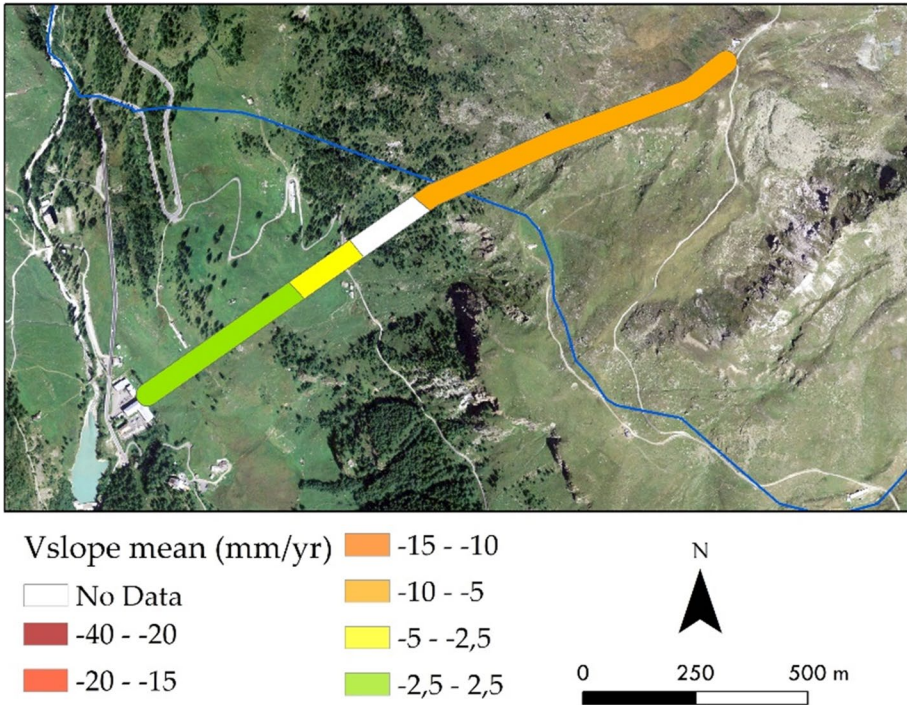
Fig. 10 Penstock of the Perrères hydroelectric plant located in the south-western limit of the MDP DsGSD subdivided into homogeneous areas based on the V_{slope} values compared in the RSAT dataset

Concerning Cielo Alto, the Sentinel-1 data, with their high temporal sampling, allowed detecting with more detail a nonlinear trend (Fig. 13A) most probably related to the seasonal thermal cycle on the tall buildings (Fig. 13B). The time series of CSK, which cover the same period of Sentinel-1, show the same trend and rate of displacement confirming the reliability of the data.

8 Discussion

In this work, the implemented methodology allowed us to develop a dedicated analysis aimed to evaluate the impacts, on structures and infrastructures, owing to large slow-moving slope instabilities evolution, combining multi-temporal SAR data, and, where available, on-site instruments measurements. Above all, multi-temporal A-DInSAR ground deformation data, covering a long-time span (about 26–28 years), have led to portraying the evolution and deformation patterns of two DsGSDs located in the Western Italian Alps, and, above all, to characterize their interferences with the main anthropic elements, highlighting the portions in which these interactions are potentially more critical. The selected DsGSDs have shown a distinct behaviour, mainly in terms of spatial homogeneity, depth of sliding surface, rate of movement and deformation trend, and also secondary landslides occurrence. This results in a variable degree of interferences with the anthropic elements
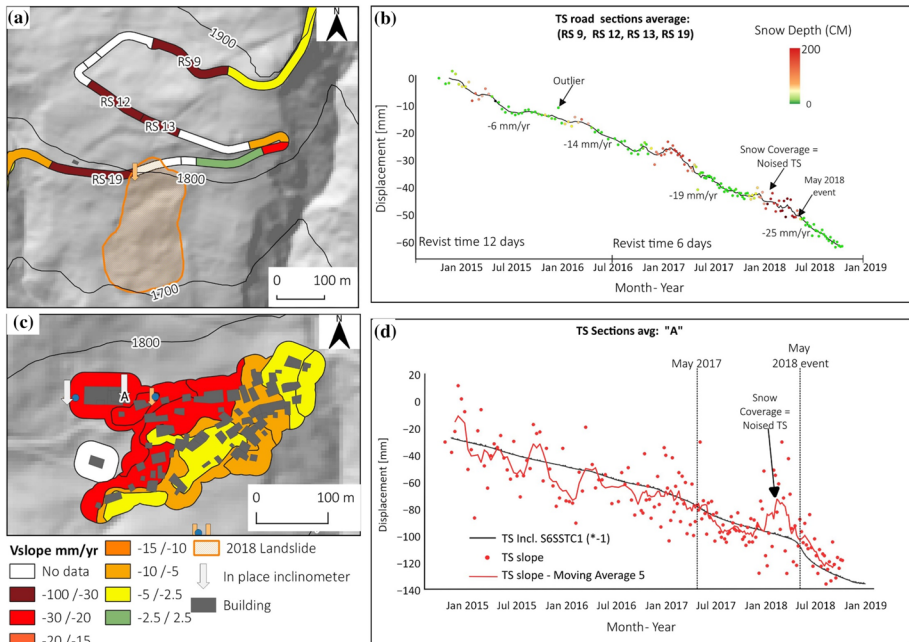
Fig. 11 **A** Location of the selected TS section along SP23 Road; **C** Location of selected TS close to inclinometer in CDC. **B** Sentinel-1 time series, the colour scale represents the snow depth (snow gauge of Sestriere located at 2000 m a.s.l. and 3 km East) at the moment of acquisition; the black line is the 3-acquisitions rolling average. D) Comparison of the inclinometer displacement time series (ARPA Piemonte 2021) with the Sentinel-1 time series project along the slope

and damage, which guarantees a good representation of the cases of interaction between DsGSDs and structures and infrastructures found on the Alpine scale.

The CDC DsGSD presents poor surficial geomorphological evidences typical of DsGSDs (e.g. trenches, double ridge, counter scarps), apart from the numerous secondary landslides associated to the DsGSD, testifying the progressive and long-term evolution of this phenomenon. In cases such as this discriminating the movement directly related to DsGSD and that associated with secondary landslides is notoriously difficult (Meisina et al. 2008; Frattini et al. 2018; Bonì et al. 2018). Through morphological evidences and previous information derived from regional landslide inventory, it is possible to identify secondary active landslide presence, discerning local movements associated to DsGSD evolution. In this case, the highest SAR displacement values were observed precisely in correspondence of the secondary landslides and in correspondence of the local sub-section in correspondence of the central portion of the DsGSD. Secondary landslides, distributed in the middle-low portion of the slope, noticeably interfere with the local road network, while the inhabited area of Champlas du Col falls in a more active sector of the DsGSD itself. This setting is well reflected by the local-scale subdivision into homogeneous sections of the main anthropic elements. The sectors with higher velocity range, based on the V_{slope} values on the diverse SAR datasets, correspond to the Champlas du Col hamlet and the adjacent two hairpin bends of the SP23 road. The ground deformation TS confirmed the strong relationship between the CDC DsGSD evolution over time for the Champlas du
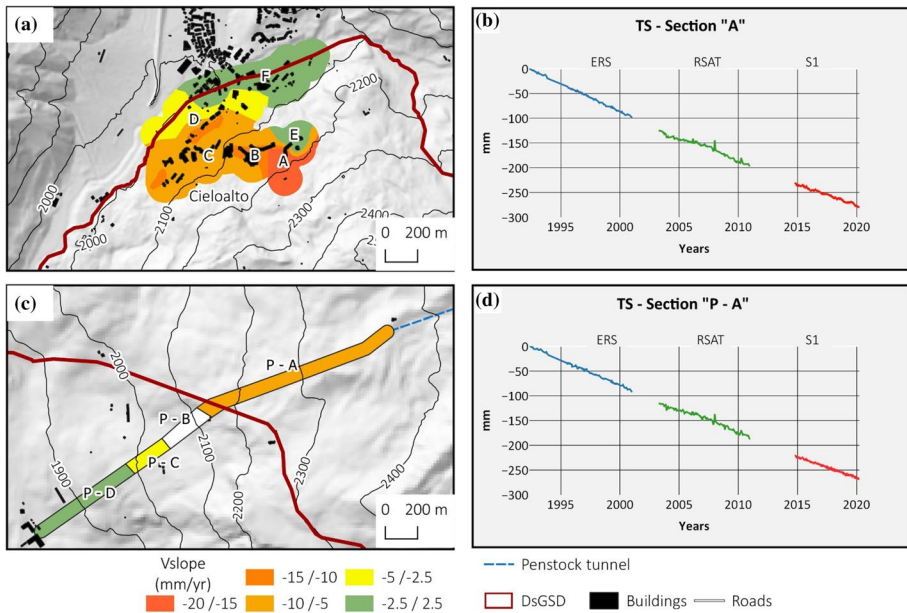
Fig. 12 Summarized Time series (1992–2020) of ERS; RSAT and Sentinel-1 for the area of Cielo Alto resort (**A**, **B**) and the penstock (**C**, **D**)

Col hamlet portion, as confirmed by the similar trend of the inclinometer measurements analysed. Instead, for the hairpin bends sector, TS analysis revealed a relationship with an early spring reactivation of a local secondary landslide, mainly due to the snow melting, as testified by the similar trend of the inclinometer data.

Compared to the CDC, the MPD case lies in correspondence of the calcschists and prasinites of the Combin Unit, and shows the typical morphostructural linear elements that characterize the DsGSD. Numerous trenches, counter scarps, elongated depressions are distributed in the upper and middle portions of this phenomenon. Another significant evidence of DsGSD evolution is represented by the rock masses fracturing, increasing downstream up to heavily broken rock masses collapsing onto themselves. This variation in rock fracturing reflects the presence of typical kinematic behaviour and a high involvement in the gravitational phenomena, most evident in the lower sector (north-east), as highlighted by the V_{slope} maps. Particularly in this sector is located the Cielo Alto hamlet, in correspondence with the highest V_{slope} values (−15 to 20 mm/year), with a linear trend movement and a cumulative displacement of about 300 mm from 1992 up to 2020. For this phenomena, the most critical sectors have been identified in correspondence with the built-up area of Cielo-Alto and along the penstock of the hydroelectric plant of Perrerès, in the southern limit of the MDP phenomena.

Therefore, through the anthropic elements characterization procedure, the identification of the most critical sectors with regard to DsGSD interaction was possible. This step allowed a spatio-temporal analysis along those most critical sectors, also accompanied by an analysis of the associated ground deformation time series. The V_{slope} maps obtained generally showed an almost constant trend over time. The projection of the average LOS velocity along the slope ensures the comparison of phenomena with diverse slopes and to homogenize data derived from different datasets. The variable orientation of phenomena
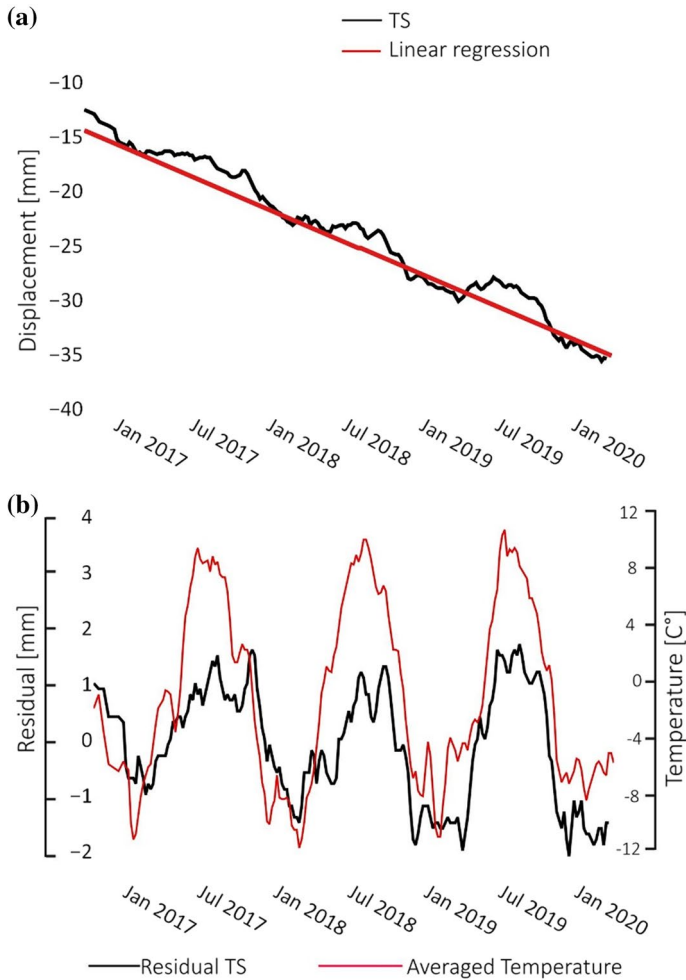
Fig. 13 **A** Focus on Sentinel-1 time series of Cielo Alto; **B** the observed residual seasonal trend compared with the monthly averaged temperature

involves some limitations in the projection of V_{LOS} along the steepest slope, especially in mountain areas due to the complex orography. Applying the post-processing procedure widely used in the literature (Bianchini et al. 2013; Notti et al. 2014; Béjar-Pizarro et al. 2017; Bonì et al. 2018; Del Soldato et al. 2019b), a certain underestimation of the real motion can be done, mainly in cases with a line-of-sight direction highly divergent from the moving direction of the observed phenomenon. Therefore, to limit this bias, some thresholds in velocity projection have been imposed, considering only PSs with $C > 0.2$ and $C < -0.2$. Because slope gradient represents another factor that may result in an underestimation, another threshold has been imposed for PSs with slope higher than 5°. Moreover, it is important to note that the risk of underestimating the velocity, particularly for NS-oriented phenomena, considering V_{LOS} values is higher than the assumption introduced projecting velocity along the slope with the above-mentioned imposed thresholds. Having considered phenomena with variable orientation (i.e. Motta de Plète ESE–WNW;

Champlas du Col mainly N–S), the proposed procedure allowed to compare deformation on diverse slopes, ensuring an overall analysis of the other DsGSDs impact on the AVR and, in general, a wider application in other mountain territories.

The numerousness of each dataset implies a certain limit to the discretization and characterization of the anthropic areas at local scale. The slight variability observed in some sections of the infrastructures is mainly attributable to the measuring points (PS/DS) distribution and coverage of the different sensors. This is particularly evident for the ERS dataset, which has a very low number of points and a rather discretized distribution, in contrast to the other datasets, as observed for instance, for the Champlas du Col hamlet area (Fig. 8) and the sectors of the SP23 in the western limit of DsGSD (Fig. 7). This variability was less evident for the anthropic elements of the MDP area, for which the number of points is decidedly higher.

This limitation should be partially overcome by considering interpolation tools commonly available in GIS environment, as already performed in Giordan et al. 2017. This would allow the prior identification of the areas most subject to the evolution of the DsGSD, through a rasterization of the data, usable as a reference base for subsequent characterization of the anthropic elements at local scale.

However, to provide an integration and a refinement of the A-DInSAR results, we have provided an additional check of the homogeneous sections delineated for the main build-up areas, comparing the ranges of V_{slope} referred to the homogeneous sectors defined for this area with the diverse degree of damage reported for each building of this village. This guarantees a valuable cross-check of the obtained results and represents a useful added value to strengthen the proposed A-DInSAR methodology with field data and information, making more effective the application of the proposed method also to other case studies. For the CDC DsGSD, we leveraged on existing data made available online (Drago et al. 2012). Overall on the four datasets, a good agreement between the severity of the damage and the V_{slope} has been observed (Fig. 14 and Supplementary material). The buildings with very severe damage, i.e. partial failure and/or disarticulation of the walls, are located in an area with high deformation rates (Fig. 14b), allowing us to identify the areas potentially most at risk.

Instead, for the Cielo-Alto area an *ad hoc* extended field survey was carried out with a punctual damage assessment on the numerous hotels and residential buildings of the Cielo-Alto hamlet. These structures, mainly characterized by linear and extended buildings, showed slight to severe damage. This high variability is potentially related to the type of building. In correspondence with reinforced concrete buildings, the damage was more evident and of a greater entity, compared to those observable in stone buildings and/or wood cladding. It should be noted that most of the buildings were under renovation, so it was not possible to properly detect the presence of damage and the related extent. Comparing V_{slope} ranges with the diverse degree of damage observed on the field for each building of the Cielo Alto hamlet, we observed that the homogeneous areas are mainly confirmed, with a distribution of the highest degree of damage in the upper part of the hamlet, up to moderate and slight damage westwards (Fig. 15 and Supplementary material). Moreover, buildings showing the highest degree of damage are related to the whole range of V_{slope} values and a remarkable amount of buildings are characterized by the absence of damage even if located in sectors with low, displacement rates. Other damage classes are evenly distributed in the highest velocity sectors.

In the area close to the main linear anthropic elements, as the hairpin bends of the SP23 of CDC area, instead, we have drawn information related to the road pavement damage (e.g. road repaving, interruption of the road), as highlighted in Cignetti et al. (2019).
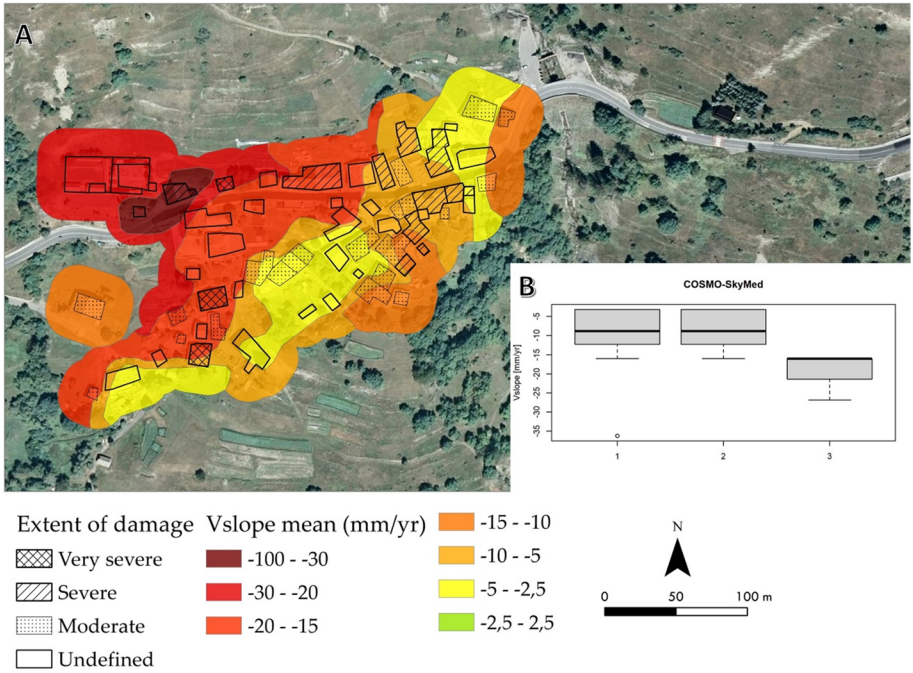
Fig. 14 Displacement map compared to building damages. The inset boxplot depicts damage classes distribution in terms of V_{slope}; moderate damage corresponds to 1, severe to 2 and very severe to 3
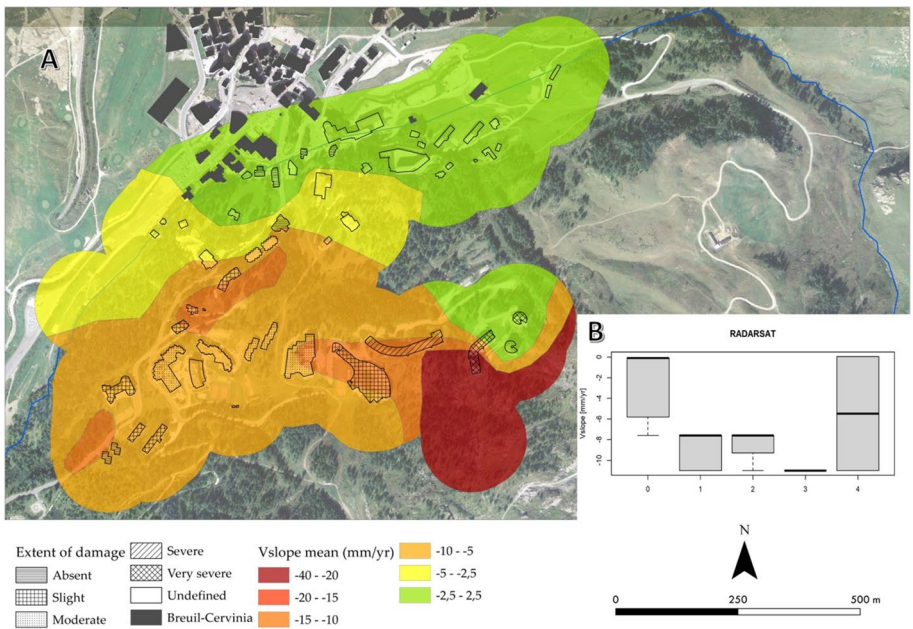

Fig. 15 **A** Displacement map compared to building damages; **B** the inset boxplot depicts damage classes distribution in terms of V_{slope} for the RSAT dataset

Instead, for the penstock of the hydroelectric plant of Perrères, it is known that the hydropower society owner of the penstock (CVA group) has been carrying out, for several years, constant maintenance in the underground stretch through the MDP DsGSD (Martinotti et al. 2011). An automated inclinometer system (Allasia et al. 2020b) monitored the penstock sector of DsGSD and confirmed the entity and direction detected by SAR data.

Overall, the implemented methodology constitutes a valid support tool for the use and post-processing of A-DInSAR data, often already available from competent administrations, allowing to distinguish sectors of strategic anthropic structures and infrastructures with higher deformation and their variation over time. This approach constitutes an effective tool for a local-scale analysis of those strategic infrastructures and inhabited areas affected by the long-term evolution of DsGSDs, pointing out those areas where targeted monitoring or maintenance is needed.

9 Conclusions

The alpine region is characterized by the presence of large areas involved by DsGSDs. As a result of their long-lasting dynamic, DsGSDs originate areas characterized by gentle slopes mainly near valley bottoms, which are ideal locations for urban settlements and strategic infrastructures. On the other hand, the aforementioned dynamic pose a threat to such anthropized areas. The slow and continuous movement of these phenomena exerts a pressure on buildings, roads and other infrastructures. The monitoring of DsGSDs and their dynamics, specifically nearby anthropic structures, infrastructures and inhabited areas that cross these huge phenomena, represent a key element in safeguarding these territories, aspects that are often neglected or underestimated compared to other landslide phenomena. A dedicated investigation of DsGSDs impact on inhabited areas and infrastructures remains a challenge and should represent a useful tool in land planning, which is currently unavailable.

Against this background, our analysis has revealed that the availability of diverse satellite-borne datasets allowed to compute displacement maps of DsGSDs over a long-time span, able to detect and distinguish sectors with different evolution and displacement rates, functional to the monitoring the evolution of these huge phenomena, both spatially and temporally. This laid the groundwork for a dedicated investigation at local scale of the main anthropic elements able to identify the effective impact of DsGSDs and the identification of those areas more affected by spatial and temporal evolution of these massive phenomena. The comparison with on-site data like GNSS surveys or surface/subsurface monitoring can further improve the campaign results by validating the results and by providing additional insights for the comprehension of the phenomenon in a broader context. Additionally, the cross-check with ground observations, like damage inventory, can support a methodology solely based on remote sensing techniques, making it more robust and applicable in other contexts.

Overall, our results and observations disclose the importance of identify the subdomains recognizable within a single DsGSD and their variable interference with anthropic structures and infrastructures, demonstrating the need and usefulness of a tool capable to monitor and characterize the interactions of these huge phenomena with the main anthropic elements aimed to a correct territorial planning and an optimized, future monitoring strategy.

Declarations

References

Agliardi F, Crosta G, Zanchi A (2001) Structural constraints on deep-seated slope deformation kinematics. Eng Geol 59:83–102. https://doi.org/10.1016/S0013-7952(00)00066-1

Agliardi F, Crosta GB, Zanchi A, Ravazzi C (2009) Onset and timing of deep-seated gravitational slope deformations in the eastern Alps, Italy. Geomorphology 103:113–129. https://doi.org/10.1016/j.geomorph.2007.09.015

Allasia P, Godone D, Giordan D et al (2020b) Advances on Measuring Deep-Seated Ground Deformations Using Robotized Inclinometer System. Sensors 20:3769. https://doi.org/10.3390/S20133769

Allasia P, Baldo M, Faccini F, et al (2020a) The role of measure of deep-seated displacements in the monitoring networks on large-scale landslide. https://doi.org/10.1007/978-3-030-60311-3_4

Ambrosi C, Crosta GB (2006) Large sackung along major tectonic features in the Central Italian Alps. Eng Geol 83:183–200. https://doi.org/10.1016/J.ENGGEO.2005.06.031

Antonielli B, Mazzanti P, Rocca A et al (2019) A-DInSAR performance for updating landslide inventory in mountain areas: an example from lombardy region (Italy). Geosciences 9:364. https://doi.org/10.3390/GEOSCIENCES9090364

Barboux C, Strozzi T, Delaloye R et al (2015) Mapping slope movements in Alpine environments using TerraSAR-X interferometric methods. ISPRS J Photogramm Remote Sens 109:178–192. https://doi.org/10.1016/J.ISPRSJPRS.2015.09.010

Barla G (2018) Numerical modeling of deep-seated landslides interacting with man-made structures. J Rock Mech Geotech Eng 10:1020–1036. https://doi.org/10.1016/j.jrmge.2018.08.006

Béjar-Pizarro M, Notti D, Mateos RM et al (2017) Mapping vulnerable urban areas affected by slow-moving landslides using Sentinel-1 InSAR data. Remote Sens 9:876. https://doi.org/10.3390/rs9090876

Berardino P, Fornaro G, Lanari R, Sansosti E (2002) A new algorithm for surface deformation monitoring based on small baseline differential SAR interferograms. IEEE Trans Geosci Remote Sens 40:2375–2383. https://doi.org/10.1109/TGRS.2002.803792

Bianchini S, Herrera G, Mateos RM et al (2013) Landslide activity maps generation by means of persistent scatterer interferometry. Remote Sens 5:6198–6222. https://doi.org/10.3390/RS5126198

Biggs J, Communications TW-N, 2020 undefined How satellite InSAR has grown from opportunistic science to routine monitoring over the last decade. nature.com

Bonì R, Bordoni M, Colombo A et al (2018) Landslide state of activity maps by combining multi-temporal A-DInSAR (LAMBDA). Remote Sens Environ 217:172–190. https://doi.org/10.1016/j.rse.2018.08.013

Bordoni M, Bonì R, Colombo A et al (2018) A methodology for ground motion area detection (GMA-D) using A-DInSAR time series in landslide investigations. CATENA 163:89–110. https://doi.org/10.1016/j.catena.2017.12.013

Bru G, González PJ, Mateos RM et al (2017) A-DInSAR monitoring of landslide and subsidence activity: a case of urban damage in Arcos de la Frontera, Spain. Remote Sens 9:787. https://doi.org/10.3390/RS9080787

Cascini L, Fornaro G, Peduto D (2010) Advanced low- and full-resolution DInSAR map generation for slow-moving landslide analysis at different scales. Eng Geol 112:29–42. https://doi.org/10.1016/j.enggeo.2010.01.003

Ciampalini A, Bardi F, Bianchini S et al (2014) Analysis of building deformation in landslide area using multisensor PSInSAR™ technique. Int J Appl Earth Obs Geoinf 33:166–180. https://doi.org/10.1016/J.JAG.2014.05.011

Cignetti M, Manconi A, Manunta M et al (2016) Taking advantage of the ESA G-POD service to study ground deformation processes in high mountain areas: a valle d'aosta case study, Northern Italy. Remote Sens 8:852. https://doi.org/10.3390/rs8100852

Cignetti M, Godone D, Wrzesniak A, Giordan D (2019) Structure from motion multisource application for landslide characterization and monitoring: the Champlas du Col Case Study, Sestriere, North-Western Italy. Sensors 19:2364. https://doi.org/10.3390/s19102364

Cignetti M, Godone D, Zucca F et al (2020) Impact of Deep-seated Gravitational Slope Deformation on urban areas and large infrastructures in the Italian Western Alps. Sci Total Environ 740:140360. https://doi.org/10.1016/j.scitotenv.2020.140360

Colesanti C, Wasowski J (2004) Satellite SAR interferometry for wide-area slope hazard detection and site-specific monitoring of slow landslides. In: Proceedings ninth international symposium on landslides, pp 795–802

Colesanti C, Wasowski J (2006) Investigating landslides with space-borne Synthetic Aperture Radar (SAR) interferometry. Eng Geol 88:173–199. https://doi.org/10.1016/j.enggeo.2006.09.013

Crippa C, Franzosi F, Zonca M et al (2020) Unraveling spatial and temporal heterogeneities of very slow rock-slope deformations with targeted DInSAR analyses. Remote Sens 12:1329. https://doi.org/10.3390/RS12081329

Crippa C, Agliardi F, Spreafico MC, et al (2019) Semi-automated regional analysis of slow-moving landslide activity and kinematics using PS-InSAR data. In: Geophysical research abstracts

Crosta GB, Frattini P, Agliardi F (2013) Deep seated gravitational slope deformations in the European Alps. Tectonophysics 605:13–33. https://doi.org/10.1016/j.tecto.2013.04.028

Del Soldato M, Di Martire D, Bianchini S et al (2019a) Assessment of landslide-induced damage to structures: the Agnone landslide case study (southern Italy). Bull Eng Geol Environ 78:2387–2408. https://doi.org/10.1007/S10064-018-1303-9/FIGURES/12

Del Soldato M, Solari L, Poggi F et al (2019b) Landslide-induced damage probability estimation coupling InSAR and field survey data by fragility curves. Remote Sens 1486(11):1486. https://doi.org/10.3390/RS11121486

Del Soldato M, Solari L, Novellino A et al (2021) A new set of tools for the generation of InSAR visibility maps over wide areas. Geoscience 11:229. https://doi.org/10.3390/GEOSCIENCES11060229

Di Martire D, Novellino A, Ramondini M, Calcaterra D (2016) A-differential synthetic aperture radar interferometry analysis of a deep seated gravitational slope deformation occurring at Bisaccia (Italy). Sci Total Environ 550:556–573. https://doi.org/10.1016/J.SCITOTENV.2016.01.102

Di Traglia F, De LC, Manzo M et al (2021) Joint exploitation of space-borne and ground-based multitemporal InSAR measurements for volcano monitoring: the Stromboli volcano case study. Remote Sens Environ 260:112441

Drago D, Sportaiuolo L, Spezzano R (2012) Schede di rilevamento danni agli edifici nei comuni di Bardonecchia e Sestriere (TO)—Deformazioni Gravitative Profonde di Versante (DGPV, Aspetti Tecnici e Normativi—Progetto RISKNAT

Ferretti A, Prati C, Rocca F (2001) Permanent scatterers in SAR interferometry. IEEE Trans Geosci Remote Sens 39:8–20

Fioraso G (2017) Impact of massive deep-seated rock slope failures on mountain valley morphology in the northern Cottian Alps (NW Italy). J Maps 13:575–587. https://doi.org/10.1080/17445647.2017.1342211

Frattini P, Crosta GB, Allievi J (2013) Damage to buildings in large slope rock instabilities monitored with the PSInSAR™ technique. Remote Sens 5:4753–4773. https://doi.org/10.3390/rs5104753

Frattini P, Crosta GB, Rossini M, Allievi J (2018) Activity and kinematic behaviour of deep-seated landslides from PS-InSAR displacement rate measurements. Landslides 15:1053–1070. https://doi.org/10.1007/s10346-017-0940-6

Giordan D, Allasia P, Manconi A et al (2013) Morphological and kinematic evolution of a large earthflow: the Montaguto landslide, southern Italy. Geomorphology 187:61–79. https://doi.org/10.1016/j.geomorph.2012.12.035

Giordan D, Cignetti M, Bertolo D (2017) The use of morpho-structural domains for the characterization of deep-seated gravitational slope deformations in valle d'aosta. In: Advancing culture of living with landslides. Springer, Cham, pp 59–68

Giordan (2006) Lo studio dei fenomeni franosi: dai sistemi informativi territoriali al monitoraggio in tempo reale. University of Turin

Godone D, Garnero G (2017) The role of morphometric parameters in Digital Terrain Models interpolation accuracy: a case study. https://doi.org/10.5721/EUJRS20134611

Gold CM (1994) Advantages of the Voronoi spatial model. In: Proceedings of the EuroCarto XII, Copenhagen, pp 1–10

Herrera G, Gutiérrez F, García-Davalillo JC et al (2013) Multi-sensor advanced DInSAR monitoring of very slow landslides: the Tena Valley case study (Central Spanish Pyrenees). Remote Sens Environ 128:31–43. https://doi.org/10.1016/j.rse.2012.09.020

Hooper A, Zebker H, Segall P, Kampes B (2004) A new method for measuring deformation on volcanoes and other natural terrains using InSAR persistent scatterers: a new persistent scatterers Method. Geophys Res Lett. https://doi.org/10.1029/2004GL021737

ISPRA CARG (2006) Carta Geologica d'Italia - Foglio 171 Cesana Torinese

ISPRA CARG (2015) Carta Geologica d'Italia—Foglio 070 Monte Cervino. http://www.isprambiente.gov.it/Media/carg/70_MONTE_CERVINO/Foglio.html

ISTAT (2019) ISTAT. https://www.istat.it/. Accessed 7 Jan 2020

Mantovani M, Bossi G, Marcato G et al (2019) New perspectives in landslide displacement detection using sentinel-1 datasets. Remote Sens 11:2135. https://doi.org/10.3390/rs11182135

Marazzi S (2005) Atlante orografico delle Alpi. SOIUSA. Priuli & Verlucca, Pavone Canavese

Martinotti G, Giordan D, Giardino M, Ratto S (2011) Controlling factors for deep-seated gravitational slope deformation (DSGSD) in the Aosta Valley (NW Alps, Italy). Geol Soc Lond Spec Publ 351:113–131. https://doi.org/10.1144/SP351.6

Meisina C, Zucca F, Notti D et al (2008) Geological interpretation of PSInSAR data at regional scale. Sensors 8:7469–7492. https://doi.org/10.3390/s8117469

Mortara G, Sorzana PF (1987) Fenomeni di deformazione graviativa profonda nell'arco alpino occidentale italiano; consideracioni lito-strutturali e morfologiche. Ital J Geosci 106:303–314

Notti D, Herrera G, Bianchini S et al (2014) A methodology for improving landslide PSI data analysis. Int J Remote Sens 35:2186–2214

Notti D, Meisina C, Zucca F, Colombo A (2011) Models to predict {Persistent} {Scatterers} data distribution and their capacity to register movement along the slope. In: Fringe workshop, pp 19–23

Pánek T, Klimeš J (2016) Temporal behavior of deep-seated gravitational slope deformations: a review. Earth Sci Rev 156:14–38. https://doi.org/10.1016/j.earscirev.2016.02.007

ARPA Piemonte (2021) GeoDissesti. http://webgis.arpa.piemonte.it/geodissesto/rercomf/grafici_tab.php?cod_strumento=S6SSTC1A-18.00,S6SSTC1B-31.00&anno=2018. Accessed 12 Oct 2021

Plank S, Singer J, Minet C, Thuro K (2012) Pre-survey suitability evaluation of the differential synthetic aperture radar interferometry method for landslide monitoring. Int J Remote Sens 33:6623–6637. https://doi.org/10.1080/01431161.2012.693646

QGIS Development Team (2009) QGIS Geographic Information System. Open Source Geospatial Foundation

Raspini F, Cigna F, Moretti S (2012) Multi-temporal mapping of land subsidence at basin scale exploiting persistent scatterer interferometry: Case study of Gioia Tauro (Italy). J Maps 8:514–524. https://doi.org/10.1080/17445647.2012.743440/SUPPL_FILE/TJOM_A_743440_SUP_29690859.PDF

Solari L, Bianchini S, Franceschini R et al (2020a) Satellite interferometric data for landslide intensity evaluation in mountainous regions. Int J Appl Earth Obs Geoinf 87:102028. https://doi.org/10.1016/j.jag.2019.102028

Solari L, Montalti R, Barra A et al (2020b) Multi-temporal satellite interferometry for fast-motion detection: an application to salt solution mining. Remote 12:3919. https://doi.org/10.3390/RS12233919

Solaro G, Acocella V, Pepe S et al (2010) Anatomy of an unstable volcano from InSAR: Multiple processes affecting flank instability at Mt. Etna, 1994–2008. J Geophys Res Solid Earth 115:10405. https://doi.org/10.1029/2009JB000820

Spreafico MC, Agliardi F, Andreozzi M, et al (2020) Large slow rock-slope deformations affecting hydropower facilities. In: EGU general assembly conference abstracts, p 8288

Trigila A, Iadanza C, Spizzichino D (2008) IFFI Project (Italian landslide inventory) and risk assessment. In: First world landslide forum, pp 18–21

Valerio E, Tizzani P, Carminati E et al (2018) Ground deformation and source geometry of the 30 October 2016 Mw 6.5 Norcia earthquake (Central Italy) investigated through seismological data, DInSAR measurements, and numerical modelling. Remote Sens 10:1901. https://doi.org/10.3390/RS10121901

Wasowski J, Pisano L (2020) Long-term InSAR, borehole inclinometer, and rainfall records provide insight into the mechanism and activity patterns of an extremely slow urbanized landslide. Landslides 17:445–457. https://doi.org/10.1007/S10346-019-01276-7/FIGURES/8

Zangerl C, Eberhardt E, Perzlmaier S (2010) Kinematic behaviour and velocity characteristics of a complex deep-seated crystalline rockslide system in relation to its interaction with a dam reservoir. Eng Geol 112:53–67. https://doi.org/10.1016/j.enggeo.2010.01.001

Authors and Affiliations

Martina Cignetti[1] · Danilo Godone[1] ⓘ · Davide Notti[1] · Francesco Zucca[2] · Claudia Meisina[2] · Massimiliano Bordoni[2] · Laura Pedretti[2] · Luca Lanteri[3] · Davide Bertolo[4] · Daniele Giordan[1]

Martina Cignetti
martina.cignetti@irpi.cnr.it

Davide Notti
davide.notti@irpi.cnr.it

Francesco Zucca
francesco.zucca@unipv.it

Claudia Meisina
claudia.meisina@unipv.it

Massimiliano Bordoni
massimiliano.bordoni@unipv.it

Laura Pedretti
laura.pedretti01@universitadipavia.it

Luca Lanteri
luca.lanteri@arpa.piemonte.it

Davide Bertolo
d.bertolo@regione.vda.it

Daniele Giordan
daniele.giordan@irpi.cnr.it

[1] National Research Council of Italy, Research Institute for Geo-Hydrological Protection (CNR IRPI), 10135 Turin, Italy

[2] Department of Earth and Environmental Sciences, University of Pavia, 27100 Pavia, Italy

[3] Dipartimento Rischi Naturali e Ambientali, ARPA Piemonte – Agenzia Regionale per la Protezione Ambientale, 10121 Turin, Italy

[4] Strutture Attività Geologiche, Regione Autonoma Valle d'Aosta, 11020 Quart, Italy